Volume 21, No 2 | International Journal of Radiation Research, April 2023

Non-invasive radiomics nomogram model for determining the low and high-grade glioma base on MRI images

S. Bijari[1], A. Jahanbakhshi[2], P. Abdolmaleki[3*]

[1]Department of Medical Physics, Faculty of Medical Sciences, Tarbiat Modares University, Tehran, Iran
[2]Stem Cell and Regenerative Research Center, Iran University of Medical Sciences, Tehran, Iran
[3]Department of Biophysics, Faculty of Biological Sciences, Tarbiat Modares University, Tehran, Iran

► ***Original article***

Corresponding author:
Parviz Abdolmaleki, Ph.D.,
E-mail: *parviz@modares.ac.ir*

Received: June 2022
Final revised: November 2022
Accepted: November 2022

Int. J. Radiat. Res., April 2023; 21(2): 275-280

DOI: 10.52547/ijrr.21.2.14

Keywords: *Glioma, low-grade glioma (LGG), high-grade glioma (HGG), radiomics, nomogram.*

ABSTRACT

***Background*:** Glioma is the most common type of tumor in the nervous system. Glioma grading remains challenging despite advancements in diagnostic and treatment systems. Preoperative classification is essential to determining optimal treatment and prognosis for gliomas. This study aimed to use magnetic resonance imaging (MRI) to develop accurate nomogram models for glioma grading. ***Materials and Methods*:** Eighty-three patients who had undergone a glioma biopsy from June 2017 to November 2021 were retrospectively collected. Two multiparametric MRIs were acquired: T2-weighted and T1-weighted gadolinium contrast-enhanced of 83 glioma patients from one medical institution. Using the open-source python package PyRadiomics, 107 radiomics features were identified for each sequence MRI. We analyzed the probabilities of low-grade gliomas (LGG) and high-grade gliomas (HGG) using logistic regression and the least absolute shrinkage and selection operator regression (LASSO). We identified seven features affecting LGG and HGG differentiated using the lasso algorithm. Next, logistic regression analysis was performed to build a classification model, and five features were obtained. Nomograms were created to predict the incidence of HGG and LLG. To evaluate the prediction performance of the models, receiver operating characteristic (ROC) curves were plotted, and the area under the curve (AUC), sensitivity, specificity, and accuracy were calculated. ***Results*:** For multivariate logistic regression models, according to the best-selected features based on MRI images and clinical data, five parameters were independent predictors of LGG from HGG (P<0.001). The highest prediction performance in terms of AUC, sensitivity, specificity, and accuracy was 0.97, 89.19%, 91.11%, and 90.24%, respectively. ***Conclusion*:** The radiomics nomogram models created from quantitative images and clinical data performed well in differentiating LGG from HGG.

INTRODUCTION

It is estimated that 30-40% of all tumors of the central nervous system (CNS) in humans are gliomas. Astrocytomas and glioblastomas are the most prevalent types of gliomas (3.21 per 100,000 and 0.46 per 100,000, respectively) [1–4]. Following WHO guidelines, there are four grades of gliomas. The consensus is that grades II and III are low-grade gliomas (LGGs), while grades IV are high-grade gliomas (HGGs). Grading determines glioma prognosis and treatment. Surgical resection is usually the primary form of postoperative treatment for LGGs, while chemotherapy and radiotherapy are commonly used for HGGs [2]. Accurate grading of gliomas is essential to improving patients' prognoses. There is also a significant association between tumor grade and postoperative recurrence rates [1–3, 5].

Following WHO categorization, a direct biopsy is the standard procedure for grading tumors. However, this method has several disadvantages, including the need for invasive procedures such as surgical resections or biopsies, sample failures caused by tumor heterogeneity, and a lengthy histological examination procedure. Brain tumors near binding sites can pose a risk during surgery [6–8].

Lambin proposed a high-throughput method for extracting and analyzing quantitative image features in 2012. In radiomics, radiological images are transformed into high-dimensional, mineable data [3, 9].

The most popular method for glioma preoperative diagnosis is an MRI scan. Gliomas may now be identified and diagnosed more precisely thanks to recent developments in MRI and multiparametric imaging [1].

The correlation between MRI multiparametric morphological features and grading has recently been studied. Computers collect quantitative data from images in radiomics. The extracted data can be used to diagnose, prognostically determine, or predict treatment response with the conversion of images

[DOI: 10.52547/ijrr.21.2.14]

into mineable databases [1, 3, 9].

Recent research suggests that MRI sequence imaging can be used to grade gliomas. Patients with gliomas often undergo MRI scans to determine their tumor type, grade, treatment response, and recurrence. Due to the difficulty of repeatedly assessing intra-tumoral heterogeneity and the limitations of sampling, histopathological studies of tumor tissue samples cannot entirely identify intra-tumoral heterogeneity. In contrast, noninvasive and regular MRIs could be performed, allowing the collection of data as the disease progresses and reducing patients' stress [10–12].

MRI examination also provides valuable information about the features and appearance of the tumor. T1c contrast-enhanced (T1w) and T2-weighted (T2w) MRI sequences are the most commonly used techniques to detect tumors. This study aimed to develop a convenient and noninvasive nomogram model method based on logistic regression and MRI radiomics (T2 weighted (T2w) and T1 weighted contrast-enhanced (T1c)) for preoperative glioma grading and improving diagnostic accuracy.

MATERIALS AND METHODS

Participants

A retrospective data analysis was performed in this investigation. The Tarbiat Modares University of Medical Science Ethics Committee approved the research procedure. (IR.MODARES.REC.1400.076).

From June 2017 to November 2021, the data of 83 patients from an 860-bed academic, research, and therapeutic hospital in Tehran, Iran were collected.

Patient records were extracted from a hospital-based registry database known as PACS. There are several major sections within the PACS system: demographic, diagnostic, therapeutic, paraclinical, history, and information. A patient who had one or more of the following characteristics was excluded from the study: patients under the age of 18 years, patients admitted for reasons other than biopsy, patients who died during hospitalization, patients discharged against medical advice, and patients with incomplete case records.

Data acquisition

Through an extensive literature review in scientific databases, the most relevant clinical features were identified. A database registry in Hazrat-e Rasool-e Akram Hospital, affiliated with the Iran University of Medical Sciences, was accessed from the finalized feature set for hospitalized patients with laboratory-confirmed brain tumors (n = 83).

A total of 83 gliomas with grades II-IV were studied: 20 with grade II, 18 with grade III (Total LGG;38), and 45 with grade IV (HGG).

Two neurosurgical specialists (SS and AJ) assessed the data, while a third researcher (DM) arbitrated any discrepancies in the interpretation between the two initial reviewers. Age, sex, location, and tumor diameter were recorded for each patient.

Tumor segmentation and radiomic feature extraction

Images were collected using a 1.5T MRI scanner at the MR Research Center (MAGNETOM Avanto, Siemens Healthineers, Erlangen, Germany). We used MR sequences consisting of T1C and T2WI. All T2 WI and T1 C pictures (matrix size: 256 × 256, slice thickness = 5 mm, and slice interval = 0 mm) were downloaded to the 3D Slicer from the image archiving and communication system (PACS). In these pictures, two radiologists with 10 years of experience (Reader 1 and 2) manually picked areas of interest (ROI) around the tumor's margin [1, 2]. ROIs were created along the tumor's edges to capture the complete tumour volume in each slice. Pyradiomics was used to preprocess pictures and extract their characteristics. Images were resampled using a voxel size of (1×1×1) and a bin width of (64). Using Pyradiomics, radiomic characteristics were retrieved from ROIs based on their three-dimensional areas of interest (3D ROIs). In all, 107 characteristics were retrieved from each sequence (table 1, supplementary) [13,14]. Training (70% of data) and validation (30% of data) were normalised using Z-scores. The repeatability of each characteristic was determined using intraobserver and interobserver intraclass correlation coefficients (ICCs) [13–15]. In order to evaluate intraobserver reliability, two readers independently segmented pictures twice each week. ICCs over 0.75 were maintained for intraobserver and interobserver characteristics. Seven classes of predictor variables were identified from the imaging dataset and analyzed [13–17].

Feature selection and radiomic signature construction

The dimension reduction for the radiomics was accomplished using the Spearman correlation analysis and the least absolute shrinkage and selection operator (LASSO) approach. The Spearman correlation coefficient was set to 0.9 to decrease feature redundancy, and the LASSO approach was adopted for feature selection, with penalty parameter tuning carried out using 10-fold cross-validation [3,9,18].

Radiomic signatures (Rad-scores) were constructed using a logistic regression model. The Rad-score is defined as the nonzero coefficient of the selected features. Using the weighted characteristics of each feature, a Rad-score was calculated for each patient[2,18,19]. Data was randomly divided into training and testing groups (n=58 and 25 respectively). Radiomics models were built using the training data.

[DOI: 10.52547/ijrr.21.2.14]

By measuring the area under the receiver operator characteristic curve (AUC), it was possible to determine the predictability of a radiomic signature.

Table 1. seven categories of predictor variables extracted from the imaged dataset.

Feature groups	Feature type
Shape features	Elongation, Flatness, LeastAxisLength, MajorAxisLength, Maximum2DDiameterColumn, Maximum2DDiameterRow, Maximum2DDiameterSlice, Maximum3DDiameter, MeshVolume, MinorAxisLength Sphericity, SurfaceArea, SurfaceVolumeRatio, VoxelVolume
First-order statistics	10Percentile, 90Percentile, Energy, Entropy, InterquartileRange, Kurtosis, Maximum, MeanAbsoluteDeviation, Mean, Median, Minimum, Range, RobustMeanAbsoluteDeviation, RootMeanSquared, Skewness, TotalEnergy, Uniformity, Variance
Gray-level dependence matrix (GLDM)	DependenceEntropy, DependenceNonUniformity, DependenceNonUniformityNormalized, DependenceVariance, GrayLevelNonUniformity, GrayLevelVariance, HighGrayLevelEmphasis, LargeDependenceEmphasis, LargeDependenceHighGrayLevelEmphasis, LargeDependenceLowGrayLevelEmphasis, LowGrayLevelEmphasis, SmallDependenceEmphasis, SmallDependenceHighGrayLevelEmphasis, SmallDependenceLowGrayLevelEmphasis
Gray-level run length matrix (GLRLM)	GrayLevelNonUniformity ,GrayLevelNonUniformityNormalized ,GrayLevelVariance ,HighGrayLevelRunEmphasis ,LongRunEmphasis ,LongRunHighGrayLevelEmphasis ,LongRunLowGrayLevelEmphasis ,LowGrayLevelRunEmphasis ,RunEntropy ,RunLengthNonUniformity ,RunLengthNonUniformityNormalized ,RunPercentage ,RunVariance ,ShortRunEmphasis ,ShortRunHighGrayLevelEmphasis ,ShortRunLowGrayLevelEmphasis
Gray-level co-occurrence matrix (GLCM)	Autocorrelation, ClusterProminence, ClusterShade, ClusterTendency, Contrast, Correlation, DifferenceAverage, DifferenceEntropy, DifferenceVariance, Inverse diference (ID), Inverse diference moment (IDM), Inverse diference moment normalized (IDMN), Inverse diference normalized (IDN), Informal measure of correlation (IMC) 1, Informal measure of correlation (IMC) 2, InverseVariance, JointAverage, JointEnergy, JointEntropy, MCC, MaximumProbability, SumAverage, SumEntropy, SumSquares
Gray-level size-zone matrix (GLSZM)	GrayLevelNonUniformity, GrayLevelNonUniformityNormalized, GrayLevelVariance, HighGrayLevelZoneEmphasis, LargeAreaEmphasis, LargeAreaHighGrayLevelEmphasis, LargeAreaLowGrayLevelEmphasis, LowGrayLevelZoneEmphasis, SizeZoneNonUniformity, SizeZoneNonUniformityNormalized, SmallAreaEmphasis, SmallAreaHighGrayLevelEmphasis, SmallAreaLowGrayLevelEmphasis, ZoneEntropy, ZonePercentage, ZoneVariance
Neighboring gray tone diference matrix (NGTDM)	Busyness, Coarseness, Complexity, Contrast, Strength

Radiomic nomogram construction

We constructed a diagnostic model using a multivariable logistic regression analysis based on the training data. The nomogram's performance was evaluated based on calibration and ROC curves [5, 11, 12, 20–22].

Statistical analysis

SPSS 22 (SPSS Inc., Chicago, Illinois, USA) and Stata 16.0 (Stata Corp., College Station, Texas, USA) were utilized to analyze the quantitative data. A Kolmogorov–Smirnov test was applied to assess the distribution of variables. A Student's t-test was employed to determine whether the unique features of LGG and HGG significantly differed for normally distributed features; otherwise, Mann-Whitney U–tests were performed. The significance level was set to $p < 0.05$. Variables that showed statistical significance in the univariate analysis were used in the multivariate analysis to predict effectiveness. All relevant predictors were included in the construction of the nomogram. Stata was used to create the nomogram and calibration graphs.

RESULTS

Demographic and clinical findings to differentiated HGG and LGG

In 83 individuals (LGG: 38, HGG: 45), gliomas were evaluated in PACS and histopathologically verified. The training and testing cohorts were randomly selected. Table 2 summarizes the important demographic and clinical features of differentiated HGG and LGG.

Table 2. Differentiated HGG and LGG based on demographic and clinical features of patients.

College	LGG	HGG	P -value
Patients	38	45	
Age (mean ±SD)	41±16	54±12	<0.01
Gender Male Female	 26 14	 24 16	0.44
Location (N) Frontal lobe Parietal lobe Temporal lobe Other locations	 22 16 1 1	 21 14 2 3	0.68
Tumors Diameter (mean ± SD)	4.6±1.8	5.4±1.6	0.03

Radiomic score and radiomic model construction

We used the scikit-learn linear Lasso model with iterative fitting along a regularization path (LassoCV) to determine the optimal value of alpha. The most appropriate model was selected using cross -validation.

A total of 107 radiomic features were extracted using the 3D Slicer. The LASSO dimension reduction and Spearman correlation analysis preserved only seven

[DOI: 10.52547/ijrr.21.2.14]

radiomic features. The importance of the seven features calculated by LASSO and the exact coefficient values are shown in figure 1 (a, b, and c).

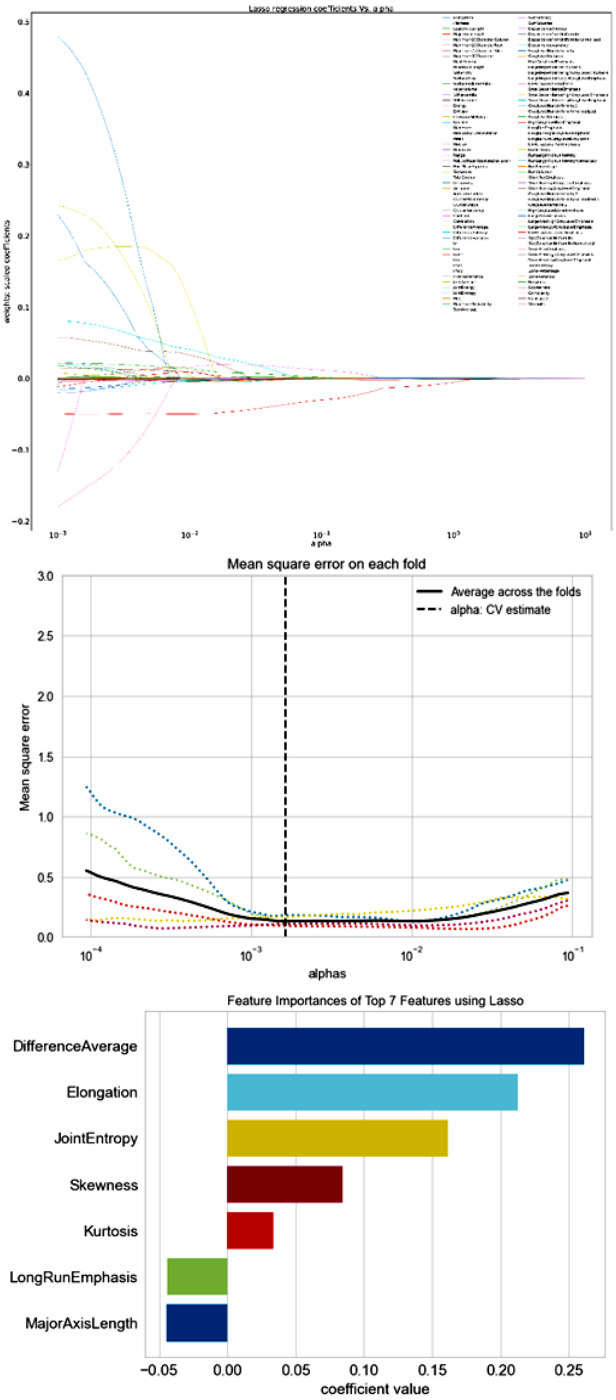

Figure 1. LASSO feature selection to separate LGG from HGG; LASSO regression was used to screen variables.

a. The coefficient profiles of the 107 characteristics were mapped to alpha. Observing the plot from left to right, we can see that the lasso models initially include a significant number of predictors with big coefficient estimates. As alpha grows, the coefficient will decrease. It is essential to remember that if alpha = 0, the lasso provides the least squares fit. If alpha is exceptionally big, the lasso yields a null model in which all coefficient estimates are 0.
b. To prevent overfitting and simplify the model, the smallest error was chosen and seven variables were maintained based on their location along the dashed line.
c. Seven variables were retained when the error was the least, based on the collected data.

Construction of the predictive nomogram

Five features were selected after the multivariable logistic regression analysis. A nomogram was created based on the findings of the multivariate analysis and the regression modeling strategies in Stata. The nomogram included important radiomic features (figure 2). The following is an example of a patient with a brain mass who scored 6.5 to 7, with a chance of GBM greater than 0.9.

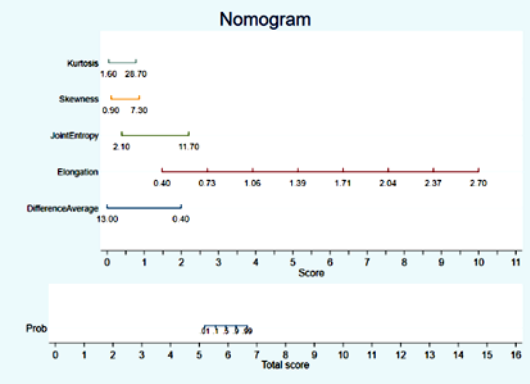

Figure 2. Nomogram result for prediction of probably HGG based on the crucial radiomic features.

Based on best-selected features based on MRI images and clinical data, the highest prediction performance with an AUC, sensitivity, specificity, and accuracy was obtained 0.97, 89.19%, 91.11%, and 90.24%, respectively. Roc curves is shown in figure 3.

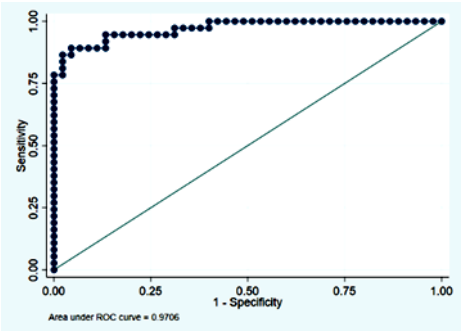

Figure 3. The predictive performance of the radiomic features and clinical data for distinguishing HGG and LGG.

For discriminating LGG from HGG, the radiomics variables provided remarkable predictive performance. For each patient in the training and testing cohorts, the calibration plot (figure 4) demonstrated considerable variation between the LGG and HGG.

[DOI: 10.52547/ijrr.21.2.14]

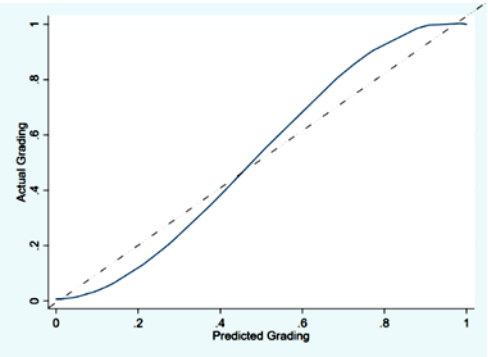

Figure 4. Calibration plot of nomogram for grading HGG and LGG(Ideal: --- -- ---).

DISCUSSION

To form a radiomic model for glioma grading, 107 characteristics were selected for each sequence. A nomogram model was used to enhance the HGG and LGG differentiation. Imaging and clinical radiomics are required to develop a prediction model. It is common for gliomas to have an abundant blood supply as high signals demonstrated in T1-W and T2-W sequences. This led us to draw an area of interest in these two sequences. Based on prior research ,to choose stable features, two physicians should perform the segmentation.

We generated seven radiomic features using the T1-C and T2-W. The features were highly predictive of preoperative LGG and HGG. On standard MR images, multiple signals and degrees of enhancement may be visible due to tumor heterogeneity. It is common for glioma signals to be confused due to intratumoral hemorrhage occurring throughout the tumor. Glioma imaging features still allow for identifying tumor enhancement with high accuracy. For the preoperative grading of glioma, MRI radiomics can provide additional information regarding the heterogeneity of the different levels of the tumor. It is also difficult to recognize with the naked eye different gray levels in glioma tumors because of their heterogeneity [23–25].

In most cases, MRI is used for preoperative diagnosis of gliomas. However, standard MRIs are often only useful for localizing tumors and evaluating them qualitatively without significantly impacting glioma grading [26–28]. However, MRI still has a limited role in preoperative grading. An increasing number of disorders are being assessed using radiomic techniques. Some researchers have applied them to different types tumors. Several studies have used similar techniques to grade gliomas [29–32]. Based on 735 images, Rathore's study revealed that the grades of gliomas differed (accuracy = 0.751, AUC = 0.652). The current study used software programs to perform a high-throughput and multidimensional texture extraction. Compared to previous models, the proposed model performs better (accuracy =0.84, AUC = 0.970), demonstrating its reliability. Cao *et al.* [33]. discovered that the location of gliomas components in the brain might discriminate between benign and malignant gliomas. The model's AUC in the training set was 0.997, but it was 0.90 in the external test set; their study was limited to morphological characteristics. Although the model performed well, the image coregistration technique must be accurate, which may restrict the model's clinical use. Takahashi *et al.* [34]. identified GBM and LGG using a machine-learning algorithm based on kurtosis and energy features on diffusion imaging. The AUC in the complete model achieved 0.98 in the external test set. However, the sample was too small, with just 55 instances. In comparison, we only employed the T2 -w MRI and T1 weighted contrast-enhanced (T1 -w +C MRI) sequences, which may have more universal applications since high-quality diffusion tensor imaging pictures may be difficult to obtain in community hospitals.

Moreover, a biopsy is crucial to determining the difference between HGG and LGG. The presented model is generalizable compared to previous research. Tumors, necrotic components, and edema zones are difficult to differentiate and segment. We segmented necrosis and edema regions which might make clinical use more viable in the future.

There are a few limitations to our research. First, experienced professionals validated the ROI of the images drawn semiautomatically. Second, the sample size was small; hence, a prospective investigation with a larger sample size is warranted. Additional research with a larger sample and validation cohorts is required to confirm our findings. Finally, the prediction model developed in this study was not externally validated, and external data should be acquired for this purpose.

CONCLUSION

The results suggest that based on the T1-C and T2 -W sequences, these radiomic models can be used as tools to differentiate LGG from HGG. According to the results of this study, radiomic nomogram models can be considered a tool to help differentiate LGG from HGG. This is more useful in patients at risk of an invasive biopsy.

ACKNOWLEDGMENT

This work was financially supported by the research department of the Tarbiat Modares University under grant number IG-39711.

Conflicts of interest: There is no conflict of interest between the authors.

Funding: No funded.

Ethical considerations: There This study was approved by the local ethics committee

[DOI: 10.52547/ijrr.21.2.14]

(IR.MODARES.REC.1400.076).

***Author contribution*:** In this paper, the following authors confirm their contributions: Salar Bijari, Amin Jahanbakhshi, and Parviz Abdolmaleki have conceived and designed the study; Salar Bijari and Amin Jahanbakhshi have collected data; Parviz Abdolmaleki and Salar Bijari have analyzed and interpreted the results; Salar Bijari has prepared a draft manuscript. The final version of the manuscript was reviewed and approved by all authors.

***Availability of data and materials*:** The datasets used and analyzed during the current study are available from the corresponding author at reasonable request.

REFERENCES

1. Wang Z, Xiao X, He K, Wu D, Pang P, Wu T (2022) A study of MRI-based machine-learning methods for glioma grading. *Int J Radiat Res, **20**(1): 115–20*.
2. Niu L, Feng WH, Duan CF, Liu YC, Liu JH, Liu XJ (2020) The value of enhanced mr radiomics in estimating the IDH1 genotype in high-grade gliomas. *Biomed Res Int, 2020*.
3. Kazerooni AF, Bagley SJ, Akbari H, Saxena S, Bagheri S, Guo J, *et al.* (2021) Applications of radiomics and radiogenomics in high-grade gliomas in the era of precision medicine. Cancers (Basel), Dec 1;13 (23).
4. Patel D, Vankawala F, Bhatt BA (2019) Survey on identification of glioblastoma multiforme and low-grade glioma brain tumor type. In: 2019 International Conference on Communication and Signal Processing (ICCSP). *IEEE, 335–9*.
5. Qi Y, Wu S, Tao L, Shi Y, Yang W, Zhou L, *et al.* (2021) Development of nomograms for predicting lymph node metastasis and distant metastasis in newly diagnosed T1-2 non-small cell lung cancer: A population-based analysis. *Front Oncol, **8**: 11*.
6. Chen C, Ou X, Wang J, Guo W, Ma X (2019) Radiomics-based machine learning in differentiation between glioblastoma and metastatic brain tumors. *Front Oncol, **9**: 806*.
7. Tateishi M, Nakaura T, Kitajima M, Uetani H, *et al.* (2020) An initial experience of machine learning based on multi-sequence texture parameters in magnetic resonance imaging to differentiate glioblastoma from brain metastases. *J Neurol Sci, **410**: 116514*.
8. Wu J, Liang F, Wei R, Lai S, Lv X, Luo S, *et al.* (2021) A multiparametric MR-based RadioFusionOmics Model with robust capabilities of differentiating glioblastoma multiforme from solitary brain metastasis. *Cancers (Basel), **13**(22): 5793*.
9. van Gómez O, Herraiz JL, Udías JM, Haug A, *et al.* (2022) Analysis of cross-combinations of feature selection and machine-learning classification methods based on [18F]F-FDG PET/CT radiomic features for metabolic response prediction of metastatic breast cancer lesions. *Cancers (Basel), **14**(12)*.
10. Duan L, Shan W, Guo L, Bo G (2022) Correlation in high resolution computed tomography signs with pathological subtype and differentiation degree of lung adenocarcinoma. *Int J Radiat Res, **20**(3): 679–85*.
11. Chen S, Wang C, Gu Y, Ruan R, Yu J, Wang S (2022) Prediction of microvascular invasion and its M2 classification in hepatocellular carcinoma based on nomogram analyses. *Front Oncol, **14**: 11*.
12. Li Y, Wu ZQ, Xu Q, Goyal H, Xu HG (2021) Development and validation of novel nomograms using serum tumor markers for the prediction of preoperative histologic grades in gastroenteropancreatic neuroendocrine tumors. *Front Oncol, **24**: 11*.
13. Bijari S, Jahanbakhshi A, Hajishafiezahramini P, Abdolmaleki P (2022) Differentiating glioblastoma multiforme from brain metastases using multidimensional radiomics features derived from MRI and multiple machine learning models. *Biomed Res Int, **2022**: 1–10*.
14. Abrigo JM, Fountain DM, Provenzale JM, *et al.* (2018) Magnetic resonance perfusion for differentiating low-grade from high-grade gliomas at first presentation. *Cochrane Database of Systematic Reviews, **2018**:(1)CD011551*.
15. Pasquini L, Jenabi M, Yildirim O, Silveira P, *et al.* (2022) Brain functional connectivity in low-and high-grade gliomas: Differences in network dynamics associated with tumor grade and location. Cancers (Basel), 14(14):3327.
16. Quazi S (2022) Artificial intelligence and machine learning in precision and genomic medicine. *Medical Oncology, **39**(8): 1–18*.
17. Bhatele KR and Bhadauria SS (2022) Machine learning application in Glioma classification: review and comparison analysis. *Archives of Computational Methods in Engineering, **29**: 247–274*.
18. Tibshirani R (2011) Regression shrinkage and selection via the lasso: a retrospective *Journal of the Royal Statistical Society Series B, **73**(3): 273-282*.
19. Chougule T, Gupta RK, Saini J, Agrawal S, *et al.* (2022) Radiomics signature for temporal evolution and recurrence patterns of glioblastoma using multimodal magnetic resonance imaging. *NMR Biomed, **35**(3): e4647*.
20. Zhang Z and Kattan MW (2017) Drawing nomograms with R: Applications to categorical outcome and survival data. *Ann Transl Med, **5**(10)*.
21. Shin MS and Lee JY (2022) Building a nomogram for metabolic syndrome using logistic regression with a complex sample—a study with 39,991,680 cases. *Healthcare (Switzerland), **10**(2)*.
22. Winter A, Kneib T, Wasylow C, Reinhardt L, *et al.* (2017) Updated nomogram incorporating percentage of positive cores to predict probability of lymph node invasion in prostate cancer patients undergoing sentinel lymph node dissection. *J Cancer, **8**(14)*.
23. Bathla G, Priya S, Liu Y, Ward C, *et al.* (2021)Radiomics-based differentiation between glioblastoma and primary central nervous system lymphoma: A comparison of diagnostic performance across different MRI sequences and machine learning techniques. *Eur Radiol, **31**(11): 8703–13*.
24. Soni N, Priya S, Bathla G (2019) Texture analysis in cerebral gliomas: a review of the literature. *American Journal of Neuroradiology, **40**(6): 928–34*.
25. Vabalas A, Gowen E, Poliakoff E, Casson AJ (2019) Machine learning algorithm validation with a limited sample size. *PLoS One, **14** (11): e0224365*.
26. Kadota Y, Hirai T, Azuma M, Hattori Y, *et al.* (2020) Differentiation between glioblastoma and solitary brain metastasis using neurite orientation dispersion and density imaging. *Journal of Neuroradiology, **47**(3): 197–202*.
27. Damon A, Clifton W, Valero-Moreno F, Quinones-Hinojosa A (2020) Cost-effective method for 3-dimensional printing dynamic multiobject and patient-specific brain tumor models. *World Neurosurg, **140**: 173–9*.
28. Mishra SK and Deepthi VH (2021) Brain image classification by the combination of different wavelet transforms and support vector machine classification. *J Ambient Intell Humaniz Comput, **12**(6): 6741–9*.
29. Yu J, Shi Z, Lian Y, Li Z, Liu T, Gao Y, *et al.* (2017) Noninvasive IDH1 mutation estimation based on a quantitative radiomics approach for grade II glioma. *Eur Radiol, **27**(8): 3509–22*.
30. Bangalore Yogananda CG, Shah BR, Vejdani-Jahromi M, *et al.* (2020) A novel fully automated MRI-based deep-learning method for classification of IDH mutation status in brain gliomas. *Neuro Oncol, **22**(3): 402–11*.
31. Lohmann P, Kocher M, Ruge MI, Visser-Vandewalle V, *et al.* (2020) PET/MRI radiomics in patients with brain metastases. *Front Neurol, **11**: 1*.
32. Kurc T, Bakas S, Ren X, Bagari A, Momeni A, Huang Y, *et al.* (2020S) egmentation and classification in digital pathology for glioma research: challenges and deep learning approaches. *Front Neurosci, **14**: 27*.
33. Shaikh F, Dupont-Roettger D, Dehmeshki J, *et al.* (2020) The role of imaging biomarkers derived from advanced imaging and radiomics in the management of brain tumors. *Front Oncol, 1807*.
34. Ortiz-Ramón R, Ruiz-España S, Mollá-Olmos E, Moratal D (2020) Glioblastomas and brain metastases differentiation following an MRI texture analysis-based radiomics approach. *Physica Medica, **76**:44–54*.

[DOI: 10.52547/ijrr.21.2.14]